Helmholtz Resonator Applied to Nanocrystal-Based Infrared Sensing

Claire Abadie, Laura Paggi, Alice Fabas, Adrien Khalili, Tung Huu Dang, Corentin Dabard, Mariarosa Cavallo, Rodolphe Alchaar, Huichen Zhang, Yoann Prado, et al.

Helmholtz Resonator Applied to Nanocrystal-based Infrared Sensing

Claire Abadie[1,2], Laura Paggi[1], Alice Fabas[1], Adrien Khalili[1,2], Tung Huu Dang[2], Corentin Dabard[2], Mariarosa Cavallo[2], Rodolphe Alchaar[2], Huichen Zhang[2], Yoann Prado[2], Nathalie Bardou[3], Christophe Dupuis[3], Xiang Zhen Xu[4], Sandrine Ithurria[4], Debora Pierucci[2], James K. Utterback[2], Baptiste Fix[1], Grégory Vincent[1], Patrick Bouchon[1], Emmanuel Lhuillier[2*]

[1] DOTA, ONERA, Université Paris Saclay, F-91123 Palaiseau, France.
[2] Sorbonne Université, CNRS, Institut des NanoSciences de Paris, 4 place jussieu, F-75005 Paris, France.
[3] Centre de Nanosciences et de Nanotechnologies (C2N), CNRS, Université Paris-Saclay, 10 Boulevard Thomas Gobert, 91120 Palaiseau, France.
[4] Laboratoire de Physique et d'Etude des Matériaux, ESPCI-Paris, PSL Research University, Sorbonne Université Univ Paris 06, CNRS UMR 8213, 10 rue Vauquelin 75005 Paris, France.

Abstract: While the integration of nanocrystals as an active medium for optoelectronic devices progresses, light management strategies become required. Over recent years, several photonic structures (plasmons, cavities, mirrors, etc.) have been coupled to nanocrystal films to shape the absorption spectrum, tune the directionality, and so on. Here, we explore a photonic equivalent of the acoustic Helmholtz resonator and propose a design that can easily be fabricated. This geometry combines a strong electromagnetic field magnification and a narrow channel width compatible with efficient charge conduction in spite of hopping conduction. At 80 K, the device reaches a responsivity above 1 $A \cdot W^{-1}$ and detectivity above 10^{11} Jones (3 µm cut-off) while offering a significantly faster time-response than vertical geometry diodes.

Keywords: photonic cavity, Helmholtz resonator, nanocrystal, infrared, photoconduction.

*To whom correspondence should be sent: el@insp.upmc.fr

In recent years, remarkable progress has been achieved in the integration of narrow band gap nanocrystals into infrared optoelectronic devices. This has enabled the demonstration of solar cells[1], light-emitting diodes[2–5] and focal plane arrays[6–8]. Using a platform such as HgTe[9,10], a wide spectral window from 1 to 5 µm can be explored with a possible extension to the long and the far infrared[11]. However, in most devices, the light-matter interaction is dictated by the electronic structure of the material itself. This has raised the need to couple the absorbing/emitting layer to a photonic structure[12] to shape the absorption[13] or enhance its magnitude[14–16]. Several concepts of photonic structures have been explored including surface plasmonics[17], a metal-insulator-metal cavity[18], optical lens[19], Fabry -Perot cavity[20], plasmonic cavity[21,22], guided mode resonator[23–25], epsilon near zero resonator[26,27], electromagnetically induced absorber[28], distributed Bragg reflector[13,29] and even the combination of some of them[14,30].

In this paper, we explore the design of an optical resonator equivalent to a Helmholtz resonator initially developed for acoustics[31], see **Figure 1**a. In this last case, a closed cavity is coupled to the external environment throughout a small opening in which the acoustic field is dramatically enhanced. The optical equivalent of this resonator has also been proposed[32], see **Figure 1**b. In the optical case, a metallic cavity confines an optical mode in a small gap where the incident light is condensed. This configuration works as an LC circuit where the cavity is an inductor and the gap acts as a capacitor. This resonator presents several advantages, such as minimizing the volume of the optically active area (*i.e.,* the gap opening) and being poorly dispersive (*i.e.,* robust toward the incident angle, which is of the utmost interest for an integration into focal plane arrays). On the other hand, the nanofabrication of the structure depicted in **Figure 1**b is challenging, requiring a simplified version[33]. Here, we demonstrate that the main properties of the initial Helmholtz resonator can be preserved in a simplified version of it, see **Figure 1**c and S1. For a full comparison of the traditional and simplified geometry of Helmholtz, see the discussion associated to Figure S5-S8. The structure presents two main differences: (*i*) the empty cavity is replaced by a dielectric layer that does not absorb light in the targeted spectral window, and (*ii*) the side walls of the cavity are removed. As a consequence, the structure has become periodic, so that the top gold layer looks like a grating with a high fill factor. Furthermore, we use the top grating as interdigitated electrodes enabling photoconductive operation for the material deposited to infill the gap. The inherent small gap between the top electrodes from the Helmholtz resonator also favors charge collection since hopping conduction is more efficient[23,34] at the scale of highly coupled grains in HgTe NC arrays.

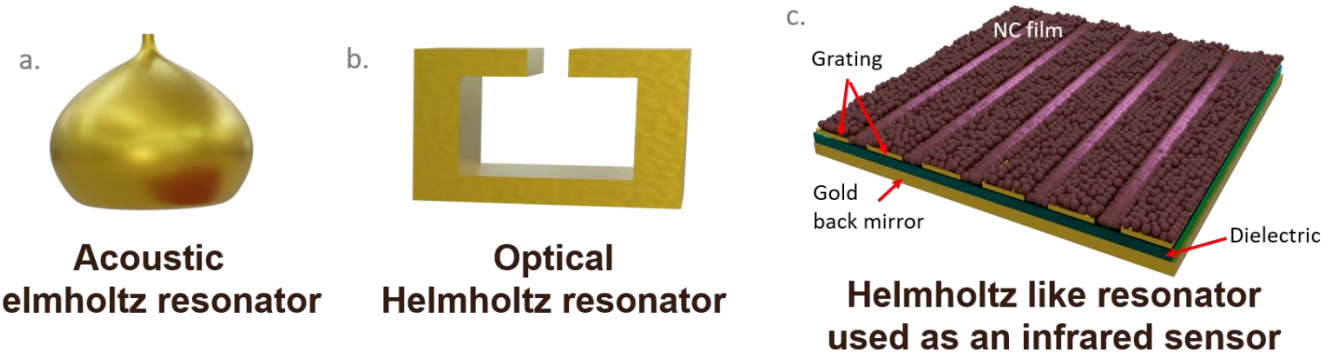

Figure 1 Helmholtz resonators. *a Schematic of a Helmholtz acoustic resonator. b. Optical equivalent for the Helmholtz resonator. c. Schematic of a Helmholtz-like resonator in which the gap is filled with infrared absorbing nanocrystals used as photoconductive medium.*

Here, we start by demonstrating that the simplified version of the resonator preserves the predicted field focusing effect of the Helmholtz resonator. We then discuss the photoconductive properties of

an infrared NC thin film used to infill the gap of the Helmholtz resonator and finally the use of such structures for light sensing in the extended short-wave infrared (2.5 µm cut-off wavelength).

To guide the design of such resonators, we used an analytical expression[32] for the resonance wavelength (λ_r) given by $\lambda_r \approx 2\pi\sqrt{\varepsilon_s \frac{h_b w_b h_s}{w_s}}$ where h_b is the dielectric height, w_b the grating period, h_s the top grating height and w_s the electrode spacing in the top grating, while ε_s is the dielectric constant of the material in the gap between the top gold electrodes. Our goal is to generate a resonance that will later match the band edge of the infrared nanocrystals used to infill the gap. According to ellipsometry measurements, the optical index of a HgTe NC film is found to be $n_s \approx 2.3$.[35] Hence, before being filled, the resonance needs to appear at $\frac{\lambda_r}{n_s} \approx 1.5\ \mu m$. We design a structure made of 28 nm of alumina, where the top grating has a thickness of 40 nm and presents a period of 350 nm with a 125 nm opening between electrodes. The structure is then built following the 4-step fabrication procedure described in Figure S9.

Without the NCs, this design generates a resonance along the transverse magnetic (TM) polarization. The latter corresponds to 75% absorption (see calculation in **Figure 2**a), assuming that there is no transmitted light in this structure thanks to the presence of a backside mirror. The transverse electric (TE) polarization, on the other hand, does not display any resonance. This analytical design is further assisted by electromagnetic simulations to unveil the electric field localization, expected to be mainly located within the electrode gap, as shown in the **Figure 2**b and S1. Note that in this simplified version of the Helmholtz resonator, the side wall of the self has been removed and this affects the electric field, which tends to leak from the gap to the dielectric layer, however this effect gets reduced once the NCs are deposited, see Figure S2-3. It is also worth pointing that the plasmonic resonance of the grating is expected to appear at $n_s.p$ with p=350 nm the period of the grating, which is expected at ≈800 nm outside of the spectral window of interest.

The dispersion map (Figure S4) shows a very weak dependence of the resonance with the planar wavevector, which can be seen as an improvement compared to similar structures based on plasmonic gratings[30] or guided mode resonators[16].

To experimentally confirm the electric field localization within the gap, we used an infrared scanning near-field optical microscope (SNOM). This near-field method can combine topography measurements with electric field magnitude measurements, see **Figure 2**c-d and S10. The electric field clearly appears more intense along lines that spatially overlap with the location of the gap on the topography map (Figure S10b), as expected from the simulations, where the field intensity is enhanced by a factor 60 in the center of the slit. This observation confirms that the simplified Helmholtz structure preserves its ability to generate an intense mode in a small volume. The full width at half maximum of this mode is around 50 nm which corresponds to $\lambda_r/26$ indicating a strong confinement of the mode. Note that in spite of its sub wavelength resolution, the SNOM resolution remains too large to resolve the two hot spots at the tip of the electrode.

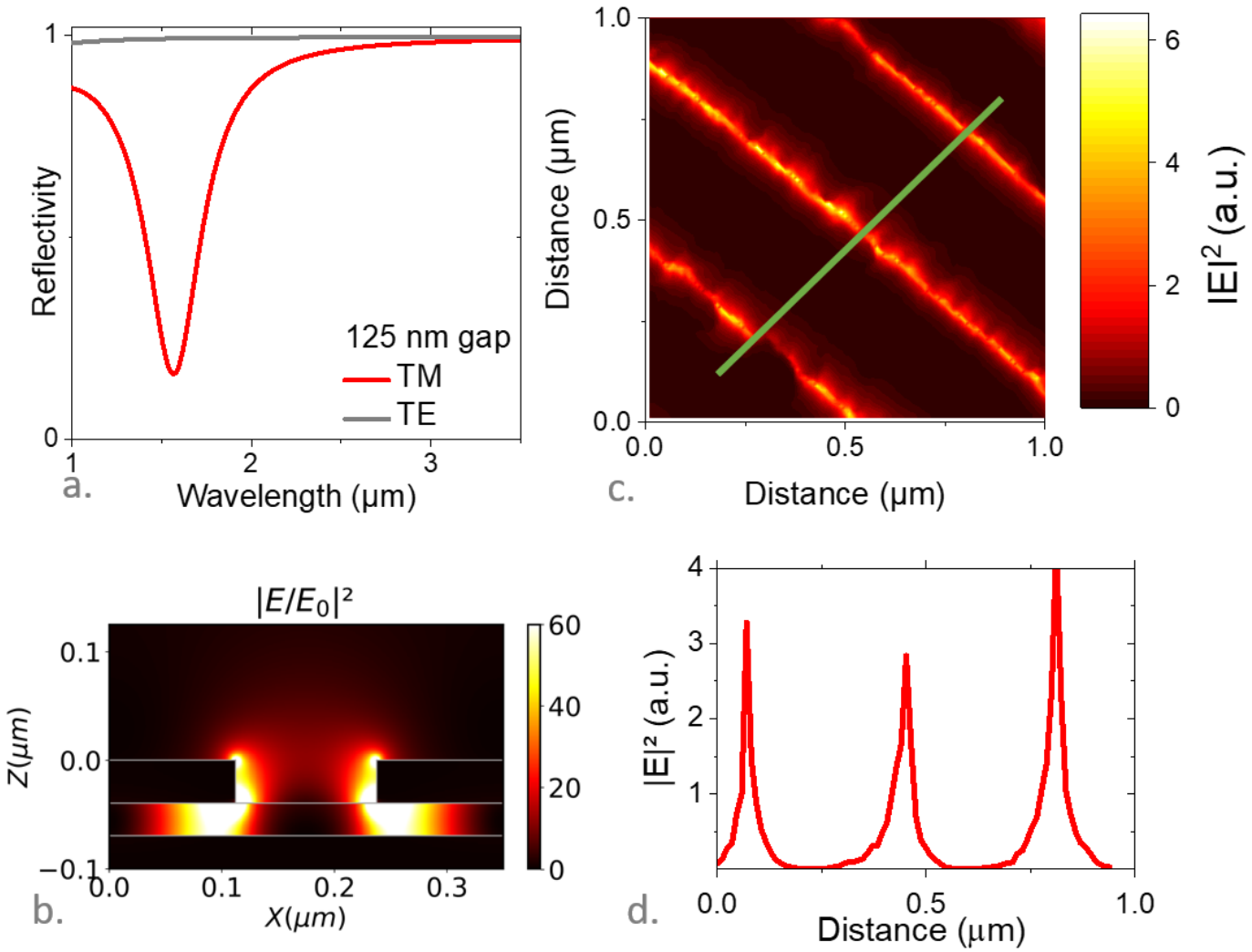

Figure 2 Resonator design without nanocrystals*. a. Simulated reflectivity spectra along the TE and TM polarization while the structure depicted in* ***Figure 1****c is not covered with NCs. The gap size is chosen to be 125 nm. b. Simulated map (side view, at 1.53 μm) of the electric field intensity enhancement factor highlighting its localization in the opening between the two electrodes. c. Map (top view) of the electric field intensity enhancement factor as measured by the SNOM at 1.55 μm and 60° of incidence. d. Profile of the intensity of the square of the electric field extracted along the green line on part c.*

We then functionalize the Helmholtz-like resonator by coating it with a photoconductive film of infrared NCs. The latter are made of HgTe and present a cut-off wavelength at 2.5 μm, as shown in **Figure 3**a. They are grown using Keuleyan's procedure[36] and present a tripodic shape[37] with a mean size around 10 nm, see the background of **Figure 3**a. The NCs are then ligand exchanged in solution using a combination of mercapthoethanol and $HgCl_2$[34,38]. This solution is then spin-coated to form a photoconductive film ≈100 nm thick. Consistent with an increase in the dielectric constant within the gap, the resonance is also shifted compared to the resonator without NCs, see **Figure 3**b and **Figure 2**a. Excellent agreements between the experimental data and the electromagnetic simulations are observed, both regarding the energy and the linewidth of the resonance. Once coated with the NCs, the Helmoltz-like resonator is expected to magnify the absorption of the material located within the gap as shown by the absorption map, see **Figure 3**c and S3 for the electric and magnetic field maps leading to 80% absorption along the TM polarization.

The benefit of the resonator is emphasized by the photocurrent spectrum. Along the TE polarization, the spectrum corresponds to the one resulting from the pristine NC film without any resonance observed, see **Figure 3**d. Along the TM polarization, the photocurrent is strongly exalted by a factor 10. Though not as high as the field magnification, this value is significantly larger than that reported for many other light resonators dedicated to absorption magnification generally reaching a 3-fold increase for plasmonic and guided mode resonators[15,16]. Upon cooling, we observe a red shift of the transition, see Figure S13. This shift has been determined to be ≈+190 μeV·K^{-1}, which matches the expected shift of the band edge for HgTe NC with a 0.5 eV interband gap value[39,40]. Beyond the shift, we also observe a broadening of the lowest energy feature at low temperature. This can be seen as the signature of the NC band edge getting detuned from the Helmholtz resonance, whose wavelength stays mostly unaffected by temperature.

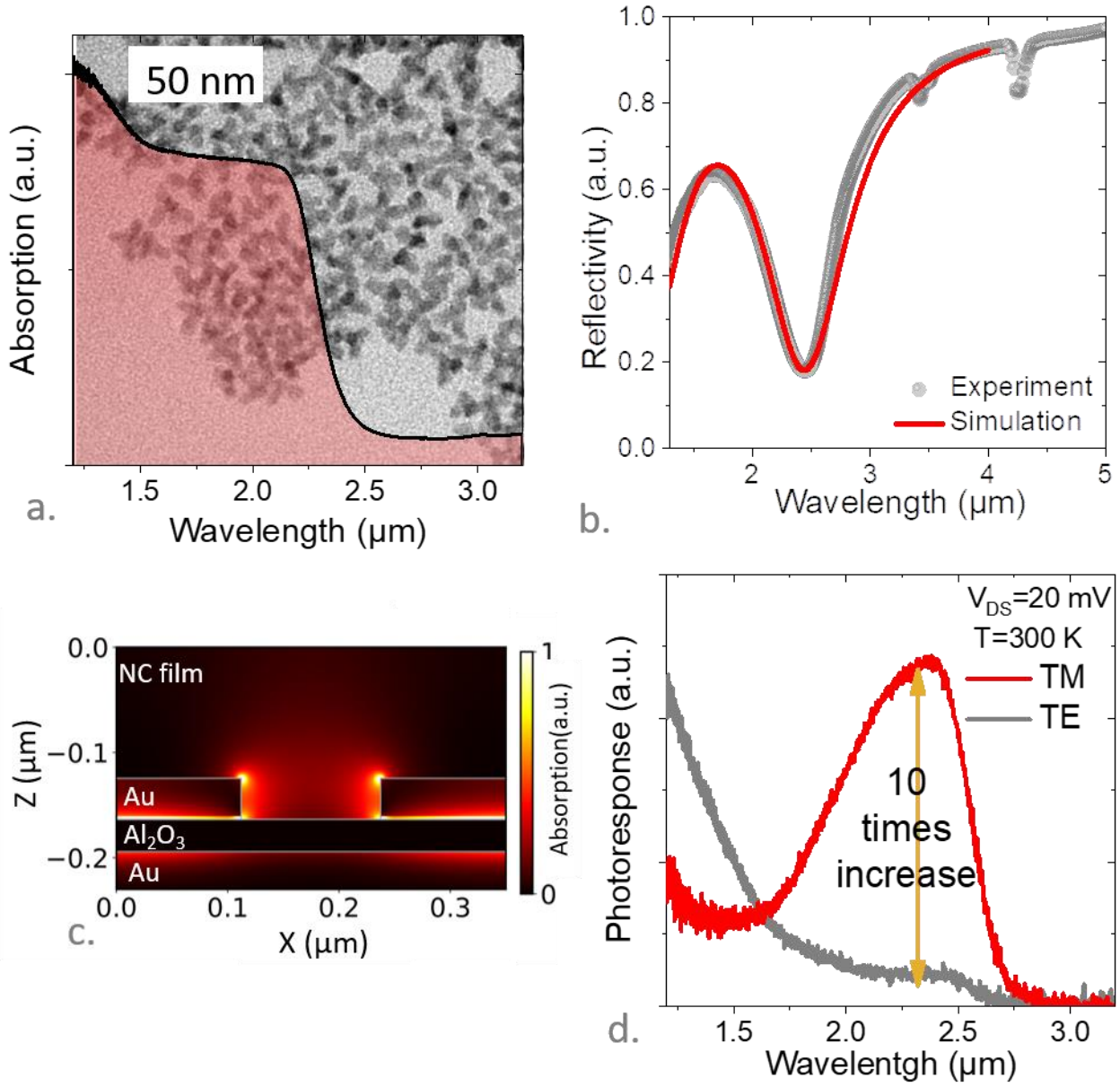

Figure 3 Spectral properties of the Helmoltz-like resonator functionalized by the NC film*. a. Absorption spectrum of the HgTe NCs used as photoconductive medium. The background is a TEM image of the same NCs. b. Experimental and simulated reflectivity spectra for the Helmoltz-like resonator functionalized by the NCs film c. Simulated map (side view) of the absorption highlighting its localization in the opening between two electrodes. d. Photocurrent spectra along TE and TM polarization, measured at room temperature under a 20 mV bias.*

In the last part of the paper, we tested the potential of this Helmholtz-like resonator for infrared sensing. The responsivity (*R*) of the film under broad band illumination (*i.e.,* blackbody radiation) starts from 100 mA·W^{-1} under low applied bias over the Helmholtz gap and can reach 5 A·W^{-1} under 500 mV (corresponding to still moderate electric field of 70 kV·cm^{-1}), see **Figure 4**a. This corresponds to an external quantum efficiency (EQE) of around $EQE = \frac{R.h.c}{e\lambda} \approx 250\%$ highlighting the presence of photoconductive gain in this structure[41], which is typical for short channel devices based on NCs[23]. In this device the noise appears to be limited by *1/f* noise[42,43], as shown in the inset of **Figure 4**b. The detectivity is moderate at room temperature around 10^8 jones. The large responsivity is also balanced by a larger dark current resulting from the short electrode spacing. Nevertheless, once the device is cooled, the dark current can drastically be reduced (Figure S12) leading to a strong increase of the signal-to-noise ratio. At 80 K, the detectivity reaches 10^{11} Jones for a cut-off wavelength almost reaching 3 µm at this temperature. Table 1 provides the infrared detection figures of merit for infrared NC films coupled to a light management strategy. The best devices in this spectral window have a detectivity in the 10^{11}-10^{12} Jones range and generally relies on a vertical diode stack, in which the dark current is also much smaller. However, thanks to its planar low capacitance geometry, our device is able to achieve a fast time-response. Under illumination by a 1.2 ns pulse at 1.57 µm, the decay time[44] has been found to be 14 ns only, see **Figure 4**c. This is at least one order of magnitude faster than the value reported for HgTe NC based photodiodes. Thus, our device offers, at cryogenic temperature, competitive performances and, in particular, a high gain bandwidth product.

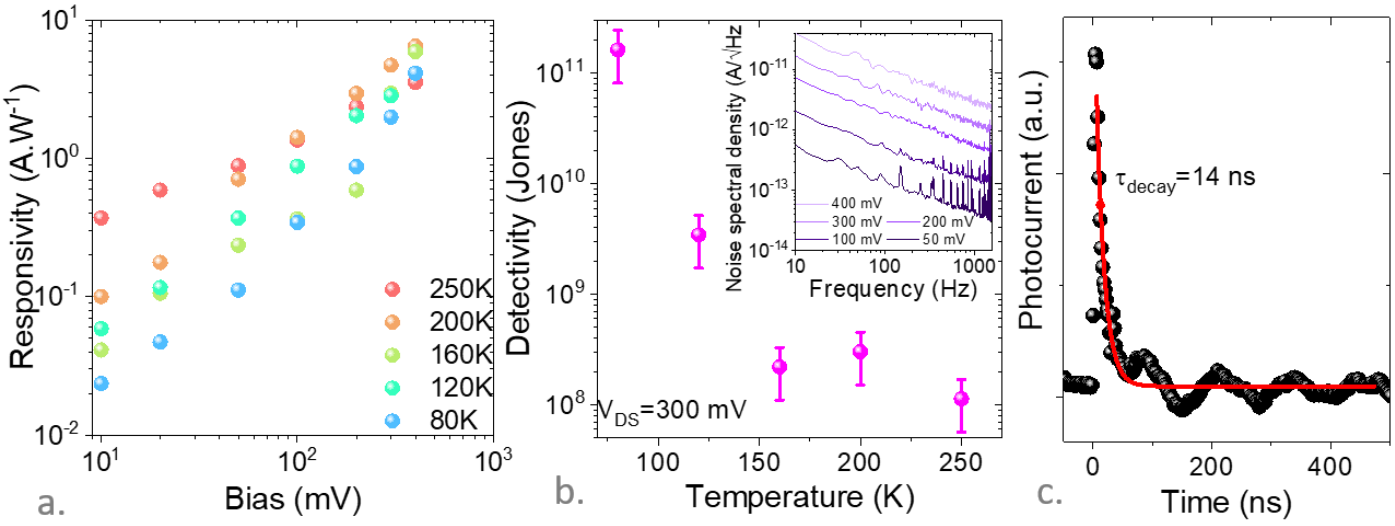

Figure 4 Infrared sensing performances for detector based on Helmoltz-like resonator. *a. Responsivity as a function of the applied bias for various operating temperatures. b. Detectivity as a function of the temperature at 300 mV for a signal frequency of 100 Hz. The inset is the spectral current density measured at 120 K under different applied biases. c. Time-response of the device after illumination by a 1.2 ns long laser pulse at 1.57 µm. Markers are experimental data, while the red line is an exponential fit.*

Table 1 Infrared detection figures of merit for infrared devices based on narrow band gap nanocrystals with a light management strategy.

Active material	**Spectral range**	**Light management strategy**	**Absorption**	**Responsivity ($A.W^{-1}$)**	**Time-response**	**Detectivity (Jones)**	**Operating temperature (K)**	**Comment - Reference**
HgTe	Visible/SWIR 0.5-1.4 µm	Gold plasmonic nanorods	- (unpolarized)	--	159 ns	1.4 $x10^{10}$	300	[22]
HgTe	MWIR 3-5 µm	Plasmonic 2D grating	20% (unpolarized)	0.02	-	1.52 $x10^{10}$	80	[15]
HgTe	MWIR 3-5 µm	Plasmonic 2D grating+Fabry Perot cavity	72% (unpolarized)	1.62	-	4 x 10^{11}	85	[14]
HgSe	MWIR-LWIR 3-10 µm	Plasmonic 2D grating	22.2% (unpolarized)	0.145	1.2 s	-	300	Very sharp FHMW (<2 µm) [21]
HgTe	SWIR 2.5 µm cut off	Fabry Perot cavity	80 % (unpolarized)	0.5	260 ns	7.5 × 10^{10}	300	Flexible device [20]
HgTe	MWIR 3-5 µm	Integrated lens	80% (unpolarized)	-	-	-	-	Theoretical work [19]
HgTe	SWIR 1.5-2 µm	Distributed Bragg mirror	100% (unpolarized)	0.2	120 ns	3 x 10^{10}	300	Ultra-narrow (30 cm^{-1}) and low loss [13]
HgTe	SWIR 2.3 µm	Metal insulator metal waveguide	78.5-95.5%	0.023	16 µs	3.2 × 10^{6}	300	On chip integrate [17]
HgTe	2.5 µm cut-off	Nanogap	0.03% (1D polarized)	1000	20 µs	10^{12}	200	[23]

PbS and HgTe	1.5 µm for PbS and 2.5 µm for Hgte	Guided mode resonator	89% (1D polarized)	1	159 µs	10^{10}	200 K	[16]
HgTe	MWIR 4 µm	GMR+MIM cavity	50% (1D polarized)	0.4	11 µs	2 x 10^{10}	80	[30]
HgTe	MWIR 3-5 µm	Plamonic grating	40% (1D polarized)	0.06	5 µs	10^{10}	80	Active platform (bias-tunable) [45]
PbS	Visible-SWIR 1.5 µm cut-off	Electromagnetically induced absorption	40% (un polarized)	-	-	-	-	[28]
HgTe	MWIR 3.5 - 4 µm	Horizontal fabry perot+vertical cavity	50 – 60 % (1D polarized)	0.07-0.3	70 ns	7x10^{10}	80	Active platform (bias-tunable) [17]
HgSe/ HgTe	SWIR MWIR 3 - 5 µm	Guided mode resonator	50 % (1D polarized)	3x10^{-3}	150 ns	10^{9}	80	Intraband transition [25]
HgTe	2.5 µm cut off	Helmholtz resonator	80% in TM (1D polarized)	5	14 ns	10^{11}	80	This work

We have designed a Helmholtz-like resonator compatible with traditional fabrication processes. This type of resonator geometry enables a high magnification (x 60) of the incident light in a small volume as confirmed by SNOM measurements. The photocurrent enhancement reaches a factor 10 while the one reported for plasmonic gratings and for guided mode resonators is generally 3 times lower. It is also worth pointing out that this enhancement is done while keeping the linewidth compatible with broadband absorption as required for imaging. Responsivity can be as high as 5 $A \cdot W^{-1}$ which is the signature of a photoconductive gain. At cryogenic temperatures, the detectivity reaches 10^{11} jones for operation under moderate bias (300 mV), while the time-response is found to be as short as 14 ns. This photonic cavity combines both a light management strategy to enhance absorption and a short channel width to be compatible with typical hopping conduction lengths, showing that efficient photoconduction properties can be obtained from highly defective films if a well-suited geometry is used.

Supporting Information

Supporting Information include (*i*) electromagnetic design, (ii) device fabrication procedure, (iii) near field microscopy, (iv) nanocrystal synthesis and transformation into photoconductive thin film.

COMPETING INTEREST

The authors declare no competing financial interests.

ACKNOWLEDEGMENTS

The project is supported by ERC starting grant blackQD (grant n° 756225). We acknowledge the use of clean-room facilities from the “Centrale de Proximité Paris-Centre”. This work has been supported by the Region Ile-de-France in the framework of DIM Nano-K (grant dopQD). This work was supported by French state funds managed by the ANR within the Investissements d'Avenir programme under reference ANR-11-IDEX-0004-02, and more specifically within the framework of the Cluster of Excellence MATISSE and also by the grants IPER-Nano2 (ANR-18-CE30-0023), Copin (ANR-19-CE24-0022), Frontal (ANR-19-CE09-0017), Graskop (ANR-19-CE09-0026), NITQuantum (ANR-20-ASTR-0008-01), Dartagnan (ANR-20-CE39-0003), Bright (ANR-21-CE24-0012-02), MixDferro (ANR-21-CE09-0029) and Quickterra (ANR-22-CE09).

REFERENCES

(1) Carey, G. H.; Abdelhady, A. L.; Ning, Z.; Thon, S. M.; Bakr, O. M.; Sargent, E. H. Colloidal Quantum Dot Solar Cells. *Chem. Rev.* **2015**, *115*, 12732–12763.

(2) Tessler, N.; Medvedev, V.; Kazes, M.; Kan, S.; Banin, U. Efficient Near-Infrared Polymer Nanocrystal Light-Emitting Diodes. *Science* **2002**, *295*, 1506–1508.

(3) Qu, J.; Weis, M.; Izquierdo, E.; Mizrahi, S. G.; Chu, A.; Dabard, C.; Gréboval, C.; Bossavit, E.; Prado, Y.; Péronne, E.; et al. Electroluminescence from Nanocrystals above 2 Mm. *Nat. Photonics* **2022**, *16*, 38–44.

(4) Pradhan, S.; Di Stasio, F.; Bi, Y.; Gupta, S.; Christodoulou, S.; Stavrinadis, A.; Konstantatos, G. High-Efficiency Colloidal Quantum Dot Infrared Light-Emitting Diodes via Engineering at the Supra-Nanocrystalline Level. *Nat. Nanotechnol.* **2019**, *14*, 72–79.

(5) Shen, X.; Peterson, J. C.; Guyot-Sionnest, P. Mid-Infrared HgTe Colloidal Quantum Dot LEDs. *ACS Nano* **2022**, *16*, 7301–7308.

(6) Kim, J. H.; Pejovic, V.; Georgitzikis, E.; Li, Y.; Kim, J.; Malinowski, P. E.; Lieberman, I.; Cheyns, D.; Heremans, P.; Lee, J. Detailed Characterization of Short-Wave Infrared Colloidal Quantum Dot Image Sensors. *IEEE Trans. Electron Devices* **2022**, *69*, 2900–2906.

(7) Greboval, C.; Darson, D.; Parahyba, V.; Alchaar, R.; Abadie, C.; Noguier, V.; Ferre, S.; Izquierdo, E.; Khalili, A.; Prado, Y.; et al. Photoconductive Focal Plane Array Based on HgTe Quantum Dots for Fast and Cost-Effective Short-Wave Infrared Imaging. *Nanoscale* **2022**, 10.1039.

(8) Liu, J.; Liu, P.; Chen, D.; Shi, T.; Qu, X.; Chen, L.; Wu, T.; Ke, J.; Xiong, K.; Li, M.; et al. A Near-Infrared Colloidal Quantum Dot Imager with Monolithically Integrated Readout Circuitry. *Nat. Electron.* **2022**, *5*, 443–451.

(9) Gréboval, C.; Chu, A.; Goubet, N.; Livache, C.; Ithurria, S.; Lhuillier, E. Mercury Chalcogenide Quantum Dots: Material Perspective for Device Integration. *Chem. Rev.* **2021**, *121*, 3627–3700.

(10) Kershaw, S. V.; Rogach, A. L. Infrared Emitting HgTe Quantum Dots and Their Waveguide and Optoelectronic Devices. *Z. Für Phys. Chem.* **2015**, *229*, 23–64.

(11) Goubet, N.; Jagtap, A.; Livache, C.; Martinez, B.; Portalès, H.; Xu, X. Z.; Lobo, R. P. S. M.; Dubertret, B.; Lhuillier, E. Terahertz HgTe Nanocrystals: Beyond Confinement. *J. Am. Chem. Soc.* **2018**, *140*, 5033–5036.
(12) Chen, M.; Lu, L.; Yu, H.; Li, C.; Zhao, N. Integration of Colloidal Quantum Dots with Photonic Structures for Optoelectronic and Optical Devices. *Adv. Sci.* **2021**, *8*, 2101560.
(13) Tang, X.; Ackerman, M. M.; Guyot-Sionnest, P. Acquisition of Hyperspectral Data with Colloidal Quantum Dots. *Laser Photonics Rev.* **2019**, *13*, 1900165.
(14) Tang, X.; Ackerman, M. M.; Guyot-Sionnest, P. Thermal Imaging with Plasmon Resonance Enhanced HgTe Colloidal Quantum Dot Photovoltaic Devices. *ACS Nano* **2018**, *12*, 7362–7370.
(15) Yifat, Y.; Ackerman, M.; Guyot-Sionnest, P. Mid-IR Colloidal Quantum Dot Detectors Enhanced by Optical Nano-Antennas. *Appl. Phys. Lett.* **2017**, *110*, 041106.
(16) Chu, A.; Gréboval, C.; Goubet, N.; Martinez, B.; Livache, C.; Qu, J.; Rastogi, P.; Bresciani, F. A.; Prado, Y.; Suffit, S.; et al. Near Unity Absorption in Nanocrystal Based Short Wave Infrared Photodetectors Using Guided Mode Resonators. *ACS Photonics* **2019**, *6*, 2553–2561.
(17) Zhu, B.; Chen, M.; Zhu, Q.; Zhou, G.; Abdelazim, N. M.; Zhou, W.; Kershaw, S. V.; Rogach, A. L.; Zhao, N.; Tsang, H. K. Integrated Plasmonic Infrared Photodetector Based on Colloidal HgTe Quantum Dots. *Adv. Mater. Technol.* **2019**, *4*, 1900354.
(18) Dhawan, A. R.; Nasilowski, M.; Wang, Z.; Dubertret, B.; Maître, A. Fabrication of Efficient Single-Emitter Plasmonic Patch Antennas by Deterministic In Situ Optical Lithography Using Spatially Modulated Light. *Adv. Mater.* **2022**, *34*, 2108120.
(19) Ning, Y.; Zhang, S.; Hu, Y.; Hao, Q.; Tang, X. Simulation of Monolithically Integrated Meta-Lens with Colloidal Quantum Dot Infrared Detectors for Enhanced Absorption. *Coatings* **2020**, *10*, 1218.
(20) Tang, X.; Ackerman, M. M.; Shen, G.; Guyot-Sionnest, P. Towards Infrared Electronic Eyes: Flexible Colloidal Quantum Dot Photovoltaic Detectors Enhanced by Resonant Cavity. *Small* **2019**, *15*, 1804920.
(21) Tang, X.; Wu, G. fu; Lai, K. W. C. Plasmon Resonance Enhanced Colloidal HgSe Quantum Dot Filterless Narrowband Photodetectors for Mid-Wave Infrared. *J. Mater. Chem. C* **2017**, *5*, 362–369.
(22) Chen, M.; Shao, L.; Kershaw, S. V.; Yu, H.; Wang, J.; Rogach, A. L.; Zhao, N. Photocurrent Enhancement of HgTe Quantum Dot Photodiodes by Plasmonic Gold Nanorod Structures. *ACS Nano* **2014**, *8*, 8208–8216.
(23) Chu, A.; Gréboval, C.; Prado, Y.; Majjad, H.; Delerue, C.; Dayen, J.-F.; Vincent, G.; Lhuillier, E. Infrared Photoconduction at the Diffusion Length Limit in HgTe Nanocrystal Arrays. *Nat. Commun.* **2021**, *12*, 1794.
(24) Gréboval, C.; Chu, A.; Magalhaes, D. V.; Ramade, J.; Qu, J.; Rastogi, P.; Khalili, A.; Chee, S.-S.; Aubin, H.; Vincent, G.; et al. Ferroelectric Gating of Narrow Band-Gap Nanocrystal Arrays with Enhanced Light–Matter Coupling. *ACS Photonics* **2021**, *8*, 259–268.
(25) Khalili, A.; Weis, M.; Mizrahi, S. G.; Chu, A.; Dang, T. H.; Abadie, C.; Gréboval, C.; Dabard, C.; Prado, Y.; Xu, X. Z.; et al. P. *ACS Photonics* **2022**, *9*, 985–993.
(26) Caligiuri, V.; Palei, M.; Imran, M.; Manna, L.; Krahne, R. Planar Double-Epsilon-Near-Zero Cavities for Spontaneous Emission and Purcell Effect Enhancement. *ACS Photonics* **2018**, *5*, 2287–2294.
(27) Caligiuri, V.; Palei, M.; Biffi, G.; Artyukhin, S.; Krahne, R. A Semi-Classical View on Epsilon-Near-Zero Resonant Tunneling Modes in Metal/Insulator/Metal Nanocavities. *Nano Lett.* **2019**, *19*, 3151–3160.
(28) Caillas, A.; Suffit, S.; Filloux, P.; Lhuillier, E.; Degiron, A. Anomalous Absorption in Arrays of Metallic Nanoparticles: A Powerful Tool for Quantum Dot Optoelectronics. *Nano Lett.* **2022**, *22*, 2155–2160.
(29) Tang, X.; Chen, M.; Ackerman, M. M.; Melnychuk, C.; Guyot-Sionnest, P. Direct Imprinting of Quasi-3D Nanophotonic Structures into Colloidal Quantum-Dot Devices. *Adv. Mater.* **2020**, *32*, 1906590.

(30) Dang, T. H.; Abadie, C.; Khalili, A.; Gréboval, C.; Zhang, H.; Prado, Y.; Xu, X. Z.; Gacemi, D.; Descamps-Mandine, A.; Ithurria, S.; et al. Broadband Enhancement of Mid-Wave Infrared Absorption in a Multi-Resonant Nanocrystal-Based Device. *Adv. Opt. Mater.* **2022**, 2200297.
(31) Hermann von Helmholtz; A Wangerin. *Theorie der Luftschwingungen in Röhren mit offenen Enden.*; W. Engelmann, 1896.
(32) Chevalier, P.; Bouchon, P.; Verdun, M.; Steveler, E.; Bardou, N.; Dupuis, C.; Pardo, F.; Haïdar, R. Experimental Demonstration of the Optical Helmholtz Resonance. *Appl. Phys. Lett.* **2018**, *112*, 171110.
(33) Fabas, A.; El Ouazzani, H.; Hugonin, J.-P.; Dupuis, C.; Haidar, R.; Greffet, J.-J.; Bouchon, P. Dispersion-Based Intertwined SEIRA and SPR Effect Detection of 2,4-Dinitrotoluene Using a Plasmonic Metasurface. *Opt. Express* **2020**, *28*, 39595.
(34) Lan, X.; Chen, M.; Hudson, M. H.; Kamysbayev, V.; Wang, Y.; Guyot-Sionnest, P.; Talapin, D. V. Quantum Dot Solids Showing State-Resolved Band-like Transport. *Nat. Mater.* **2020**, *19*, 323–329.
(35) Rastogi, P.; Chu, A.; Dang, T. H.; Prado, Y.; Gréboval, C.; Qu, J.; Dabard, C.; Khalili, A.; Dandeu, E.; Fix, B.; et al. Complex Optical Index of HgTe Nanocrystal Infrared Thin Films and Its Use for Short Wave Infrared Photodiode Design. *Adv. Opt. Mater.* **2021**, *9*, 2002066.
(36) Keuleyan, S.; Lhuillier, E.; Guyot-Sionnest, P. Synthesis of Colloidal HgTe Quantum Dots for Narrow Mid-IR Emission and Detection. *J. Am. Chem. Soc.* **2011**, *133*, 16422–16424.
(37) Chee, S.-S.; Gréboval, C.; Magalhaes, D. V.; Ramade, J.; Chu, A.; Qu, J.; Rastogi, P.; Khalili, A.; Dang, T. H.; Dabard, C.; et al. Correlating Structure and Detection Properties in HgTe Nanocrystal Films. *Nano Lett.* **2021**, *21*, 4145–4151.
(38) Martinez, B.; Ramade, J.; Livache, C.; Goubet, N.; Chu, A.; Gréboval, C.; Qu, J.; Watkins, W. L.; Becerra, L.; Dandeu, E.; et al. HgTe Nanocrystal Inks for Extended Short-Wave Infrared Detection. *Adv. Opt. Mater.* **2019**, *7*, 1900348.
(39) Moghaddam, N.; Gréboval, C.; Qu, J.; Chu, A.; Rastogi, P.; Livache, C.; Khalili, A.; Xu, X. Z.; Baptiste, B.; Klotz, S.; et al. The Strong Confinement Regime in HgTe Two-Dimensional Nanoplatelets. *J. Phys. Chem. C* **2020**, *124*, 23460–23468.
(40) Lhuillier, E.; Keuleyan, S.; Guyot-Sionnest, P. Optical Properties of HgTe Colloidal Quantum Dots. *Nanotechnology* **2012**, *23*, 175705.
(41) Konstantatos, G.; Sargent, E. H. PbS Colloidal Quantum Dot Photoconductive Photodetectors: Transport, Traps, and Gain. *Appl. Phys. Lett.* **2007**, *91*, 173505.
(42) Liu, H.; Lhuillier, E.; Guyot-Sionnest, P. 1/f Noise in Semiconductor and Metal Nanocrystal Solids. *J. Appl. Phys.* **2014**, *115*, 154309.
(43) Lai, Y.; Li, H.; Kim, D. K.; Diroll, B. T.; Murray, C. B.; Kagan, C. R. Low-Frequency (1/ *f*) Noise in Nanocrystal Field-Effect Transistors. *ACS Nano* **2014**, *8*, 9664–9672.
(44) Schedel, C.; Strauß, F.; Scheele, M. Pitfalls in Determining the Electrical Bandwidth of Nonideal Nanomaterials for Photodetection. *J. Phys. Chem. C* **2022**, *126*, 14011–14016.
(45) Dang, T. H.; Vasanelli, A.; Todorov, Y.; Sirtori, C.; Prado, Y.; Chu, A.; Gréboval, C.; Khalili, A.; Cruguel, H.; Delerue, C.; et al. Bias Tunable Spectral Response of Nanocrystal Array in a Plasmonic Cavity. *Nano Lett.* **2021**, *21*, 6671–6677.

TOC graphic

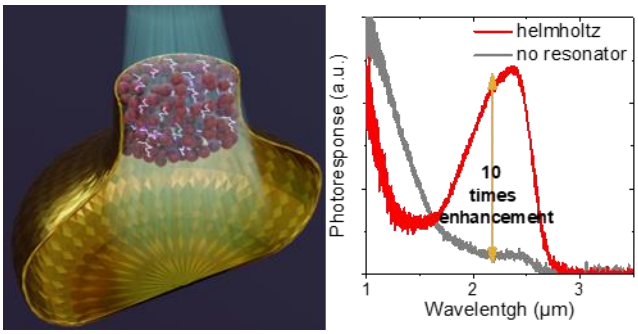
helmholtz
no resonator
Photoresponse (a.u.)
10
times
enhancement
1
2
3
Wavelentgh (μm)